ADVANCED ENGINEERING MATERIALS
www.aem-journal.com

CeO_2 Nanostructures Prepared by Selective Water-Soluble $Sr_3Al_2O_6$(SAO)-CeO_2 Vertically Aligned Nanocomposite

*Benson Kunhung Tsai, Jialong Huang, Jianan Shen, Yizhi Zhang, James P. Barnard, Claire A. Mihalko, Abhijeet Choudhury, Shiyu Zhou, and Haiyan Wang**

The unique redox properties and high oxygen capacity of nanostructured CeO_2 demonstrate a wide range of applications, such as electrolytes for solid oxide fuel cells, gas sensors, and catalysis for automotive exhaust gas. Most CeO_2 nanomaterials are prepared by chemical synthesis or hard templating methods. An effective way to obtain highly textured, small-radius dimensions with high specific surface area remains challenging. Here, highly textured CeO_2 nanostructures with various shapes ranging from nanowires to nanoporous thin films are successfully synthesized. Vertically aligned nanocomposites (VANs) of $Sr_3Al_2O_6$ (SAO) and CeO_2 are synthesized first while varying concentration ratio between them. Once the SAO is dissolved in water, the remaining CeO_2 forms distinct nanostructures. The thermal stability of the nanostructured CeO_2 is evaluated by *in situ* heating XRD and thermal annealing tests. This method provides an alternative approach to preparing nanostructured CeO_2 without toxic chemical solutions or complex micro/nanofabrication techniques. These results present a novel approach to prepare nanostructured CeO_2 for future sensing and energy device applications.

1. Introduction

High specific surface area nanomaterials are crucial for many applications, such as gas storage, electrocatalysts, and supercapacitors. Lower-dimension, such as 2D or 1D, nanomaterials result in a larger specific surface area than 3D films.[1] Nowadays, there are multiple ways to prepare high surface area films using either a top-down[2] or bottom-up approach.[3] Bottom-up approaches include vapor deposition methods[4] and templated methods to grow low-dimensional materials,[5] for instance, using chemical vapor deposition to grow various shapes of nanowires and 2D materials. Another example is utilizing an anodized alumina template to grow materials in nanowire-like shapes. Recently, a selective etching method with a vertically aligned nanocomposite (VAN) template provides an alternative solution to obtain highly textured nanoporous thin films with pores smaller than 10 nm.[3,6] Therefore, an alternative solution was provided to develop a low-dimensional and high specific area nanomaterials for future applications.

Low-dimensional metal oxide materials show versatile physical properties and notable results in various applications. Among all the oxide materials, cerium (IV) oxide (CeO_2) is one of the most important rare earth materials and has received much attention. CeO_2 has a high oxygen capacity and a unique redox property. Its unique properties lead to a wide range of applications, such as oxygen promoters for automotive exhaust,[7] electrolyte for solid oxide fuel cell,[8] and gas sensors.[9] To prepare polycrystalline CeO_2 nanostructure, different chemical synthesis approaches have been developed.[10] Alternatively, a hard template method have been implemented for obtaining the CeO_2 nanowire.[11] The diameter of the CeO_2 is limited by the size of the AAO template, which is usually larger than 10 nm.[5] Thus, developing a method to obtain a small dimension and highly crystalline nanostructured CeO_2 is essential.

VAN is a thin film with a unique nanopillar-in-matrix form, which has attracted a lot of attention recently.[12] Such nanostructures provide multifunctionality,[13] strong interfacial coupling,[14] and anisotropic properties.[15] Various material combinations can form VANs, such as oxide-oxide VANs, oxide-metal VANs, and nitride-metal VANs. Furthermore, the nanostructures can be tuned by changing simple parameters such as laser frequency,[16] thickness,[15] and material selections.[13,17] Tuning different synthesis parameters will result in different sizes of nanopillars[18] and various pillar densities,[19] as well as a range of nanostructures from 1D to other unique configurations.[20] Such tunability provides an opportunity to use VAN as a template to further design nanostructures.

B. Kunhung Tsai, J. Huang, J. Shen, Y. Zhang, J. P. Barnard, C. A. Mihalko, A. Choudhury, S. Zhou, H. Wang
School of Materials Engineering
Purdue University
West Lafayette, Indiana 47907, USA
E-mail: hwang00@purdue.edu

H. Wang
School of Electrical and Computer Engineering
Purdue University
West Lafayette, Indiana 47907, USA

The ORCID identification number(s) for the author(s) of this article can be found under https://doi.org/10.1002/adem.202500530.

DOI: 10.1002/adem.202500530

In this work, a novel approach is developed to synthesize various CeO_2 nanostructures. Specifically, a new $Sr_3Al_2O_6$ (SAO)-CeO_2 VAN system was synthesized. SAO-CeO_2 VAN system was selected to grow on an $SrTiO_3$ substrate that satisfies the strain compensation model for the desired VAN morphology.[21] In addition, varying the target concentration ratio between CeO_2 and SAO can result in different morphologies of nanostructured CeO_2. After dissolving the SAO with water, nanostructured CeO_2 can be obtained. The overall process to obtain different CeO_2 nanostructures is schematically shown in **Figure 1**. Furthermore, the thermal stability of these different CeO_2 nanostructures has also been investigated by *in situ* heating XRD and post-annealing XRD. Nanostructure tuning and thermal stability are important for future applications that require high temperature operations.

2. Results and Discussion

To satisfy the strain compensation theory for the growth of the VAN, the lattice parameter must first be examined.[20] It is known that CeO_2 ($a = 5.411$ Å) will result in a 45° rotation when it grows on the STO ($a = 3.905$ Å) substrate; thus, the lattice parameter should be considered as $a/\sqrt{2} = 3.83$ Å.[22] The lattice parameter for the SAO is $a = 15.833$ Å, which is slightly larger than the $4 \times a_{STO} = 15.620$ Å.[23] Figure S1 in Supporting Information, shows a schematic illustration of the growth relationship, where the SAO should be in a cube-on-cube relationship, and CeO_2 has a 45° rotation to grow on STO. Since the SAO lattice parameter is slightly higher than that of STO ($4 \times a_{STO}$) and the lattice of CeO_2 after the 45° rotation is slightly smaller than STO, the in-plane strain between SAO and CeO_2 satisfy the strain compensation model.[18] The nanostructure of the thin film has been examined first and is presented in Figure S2, Supporting Information. Figure S2a in Supporting Information, shows the XRD result of the SAO-CeO_2 VAN thin film before dissolving. A high resolution XRD in Figure S2b, Supporting Information, confirmed the SAO peak is not shown in the XRD pattern, which might be due to low intensity. In addition, the CeO_2 (002) and CeO_2 (004) peaks are present in the XRD pattern. The following scanning transmission electron microscopy (STEM) image in Figure S2c, Supporting Information, confirms the formation of the SAO-CeO_2 VANs. The corresponding STEM-EDS mapping in Figure S2d, Supporting Information, provides additional support for the formation of the SAO-CeO_2 VAN. After dissolving the thin film in deionized (DI) water, the XRD in Figure S2a, Supporting Information, reveals that there are no additional peaks besides the STO (001) substrate. This suggests that the nanostructured CeO_2 may have been washed off as previously demonstrate in SAO-Au VAN.[24] Thus, a thin buffer layer of CeO_2 was deposited to ensure the nanostructured CeO_2 remains after the water dissolution process. Three different targets with different ratios between SAO and CeO_2 were used to synthesize SAO-CeO_2 VAN. The target ratios of CeO_2 are 30 wt.%, 50 wt.%, and 70 wt.%. The XRD results for all three different ratios of SAO-CeO_2 are shown in **Figure 2**. Figure 2a–c shows the nanostructure thin film before dissolution. Unlike the XRD results without a CeO_2 buffer layer, the 50 wt.% CeO_2 and 70 wt.% CeO_2 show the SAO (00 12) peak. This indicates that the SAO-CeO_2 VAN may form even after inserting the CeO_2 buffer layer. The additional selected area diffraction pattern (SAED) has also shown similar crystallinity result for all three samples before dissolution as shown in Figure S3, Supporting Information. The SAED shows highly textured growth of CeO_2 on the STO substrate. The typical 45° rotation of CeO_2 is shown in the SAED pattern as well.[25] Furthermore, after all thin film were placed in DI water for 12 h, the CeO_2 peaks remained as shown in Figure 2d–f. Thus, the nanostructure of CeO_2 remains on top of the buffer layer, where the AFM and STEM images in Figure S4 and S5, Supporting Information, support the result.

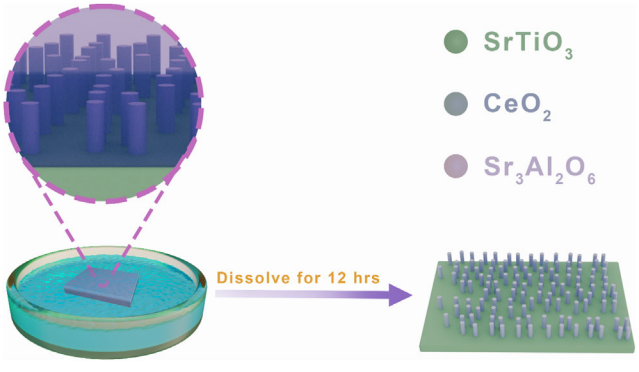

Figure 1. Schematic illustration of formation of a CeO_2 nanostructure by selective dissolution of $Sr_3Al_2O_6$.

To better understand the nanostructure and elemental distribution before dissolving SAO, STEM and STEM-EDS were performed. All STEM images were taken under the high-angle annular dark field (HAADF) mode. The cross-sectional image for all three thin films is shown in **Figure 3**. Figure 3b,e,h, where VAN is formed for all concentrations. To examine the nanostructure more closely, a zoomed-in view for all ratios of concentration is shown in Figure 3. The top and the bottom of the film have been examined by HADDF-STEM to ensure the nanostructure is attached to CeO_2 buffer layer. The SAO cannot be revealed with high magnification HAADF-STEM images that are shown in Figure 3, which may be caused by the electron beam damaged. Additionally, Figure S6, Supporting Information, clearly shows the corresponding CeO_2 is slightly bent during scanning STEM-EDS signal, which confirms the SAO can be damaged. To confirm the elemental distribution of nanostructure for the VAN, STEM-EDS images for all three concentrations are shown in Figure S6, Supporting Information. All images show a clear elemental distribution where the Al and Ce are well-separated, which confirms VAN has formed. To further confirm CeO_2 nanostructure, a plan-view sample for all concentrations was prepared. The resulting HAADF-STEM images and corresponding STEM-EDS are shown in **Figure 4**. At the lowest concentration of SAO-CeO_2, the CeO_2 nanostructure shows a rounded shape. As the concentration ratio of CeO_2 increases in target composition, a squarish-like CeO_2 appearance is shown. When CeO_2 dominates the concentration within the film, it becomes a rounded maze-like structure. To further confirm the amount of CeO_2 within the films, the atomic fraction of the sample from plan-view EDS, which are 1.42%, 2.98%, and

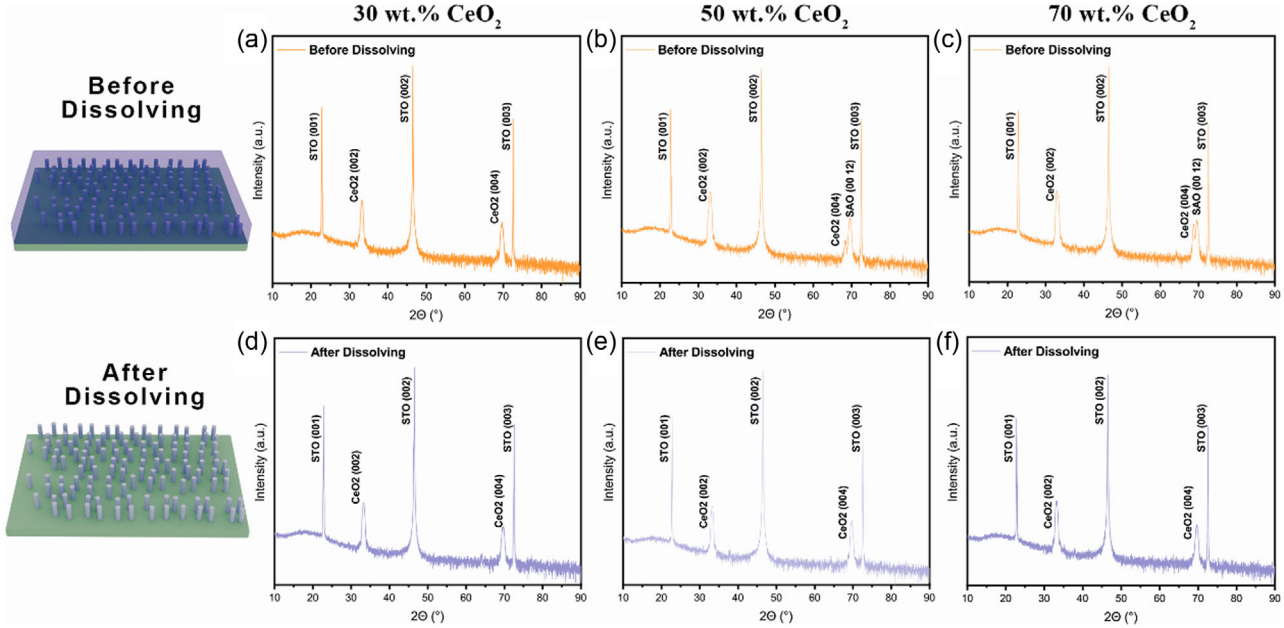

Figure 2. XRD characterization of the samples before and after water dissolution process. a–c) Before dissolving SAO. (a) 30 wt.% CeO_2, (b) 50 wt.% CeO_2, and (c) 70 wt.% CeO_2. d–f) after dissolving SAO. (d) 30 wt.% CeO_2, (e) 50 wt.% CeO_2, and (f) 70 wt.% CeO_2.

10.55% correspond to 30%wt, 50%wt, and 70%wt of CeO_2 in the SAO-CeO_2 target. Overall, the planview and cross section view of HAADF-STEM with corresponding STEM-EDS images shows different nanostructure of SAO-CeO_2 VAN ranging from nanopillar to rounded maze CeO_2.

After the nanostructure of SAO-CeO_2 VAN was examined, the nanostructure of CeO_2 after the water dissolution process was examined as well. **Figure 5** shows the cross-sectional HAADF-STEM images of the nanostructures after the water dissolution of 50 wt.% CeO_2. Instead of observing completely straight CeO_2 nanowires remaining on the top of the substrate, a slight difference in the CeO_2 nanostructures was observed. The remaining CeO_2 nanowires had agglomerated into an island-like structure. Such agglomeration may be caused by the mechanical instability for the high-aspect ratio of the nanowires. After zooming into the area of interest, the nanostructured CeO_2 maintained its own structure after the water dissolution process. The corresponding STEM-EDS image is shown in Figure S6, Supporting Information, which clearly indicates the CeO_2 nanowires agglomerates. Since the PLD is known to have difficulty in obtaining large area thin film, the SAO-CeO_2 was deposited on a 5 mm × 10 mm STO (001) substrate. Different areas of the substrate have been examined by HAADF-STEM with corresponding STEM-EDS shown in Figure S7, Supporting Information. The resulting figures suggest that the film with different areas has similar nanostructures after the dissolution process. To understand the plan view of the agglomerated nanostructure, additional AFM images are shown in Figure S4, Supporting Information, to illustrate the overall nanostructure after the water dissolution process with different concentrations of CeO_2. The AFM images show that the higher concentration of CeO_2 has larger island-like agglomeration of CeO_2 nanowires than those in 30 wt.% and 50 wt.% CeO_2. The 70 wt.% sample shows more maze-like structure in the planview STEM images before water dissolution. After evaluating the nanostructures in STEM, STEM-EDS, and AFM, the results clearly confirm that the nanostructured CeO_2 has remained on the STO substrate.

Nanostructured CeO_2 has been widely adopted in different applications, such as gas sensor[26] and electrolyte for solid oxide fuel cell.[27] All these applications require operation at a high temperatures for optimal performance. An additional temperature-dependent optical test was performed to observe if there is any optical difference under high temperature. First, Figure S10a, Supporting Information, shows a temperature-dependent *in situ* XRD with one cycle of heating and cooling from room temperature to 800 °C. The minor left shift of CeO_2 (002) when the temperature rises, which is due to the thermal expansion of the lattice. After cooling to room temperature, the peak shifts back to its original position. Overall, the *in situ* heating XRD suggests the CeO_2 nanostructure is relatively thermally stable during the *in situ* heating test. Additionally, different concentrations of nanostructure CeO_2 thin films were annealed under 1000 °C. The resulting XRD for the before and after annealing sample indicated the CeO_2 may potentially stay on the substrate as shown in Figure S8, Supporting Information. Furthermore, the CeO_2 nanostructure after annealing is shown in Figure S9, Supporting Information. The resulting nanostructure shows different nanostructure compared to the initial agglomerated nanowire. This might be due to the thermal agglomeration.[28] Next, the optical permittivity at room temperature and elevated temperature was investigated, which are shown in Figure S10, Supporting Information. Figure S10b, Supporting Information, shows the real part of room temperature optical permittivity where the in-plane and out-of-plane show positive values from 500 to 2500 nm. This indicates the entire film is an insulator.

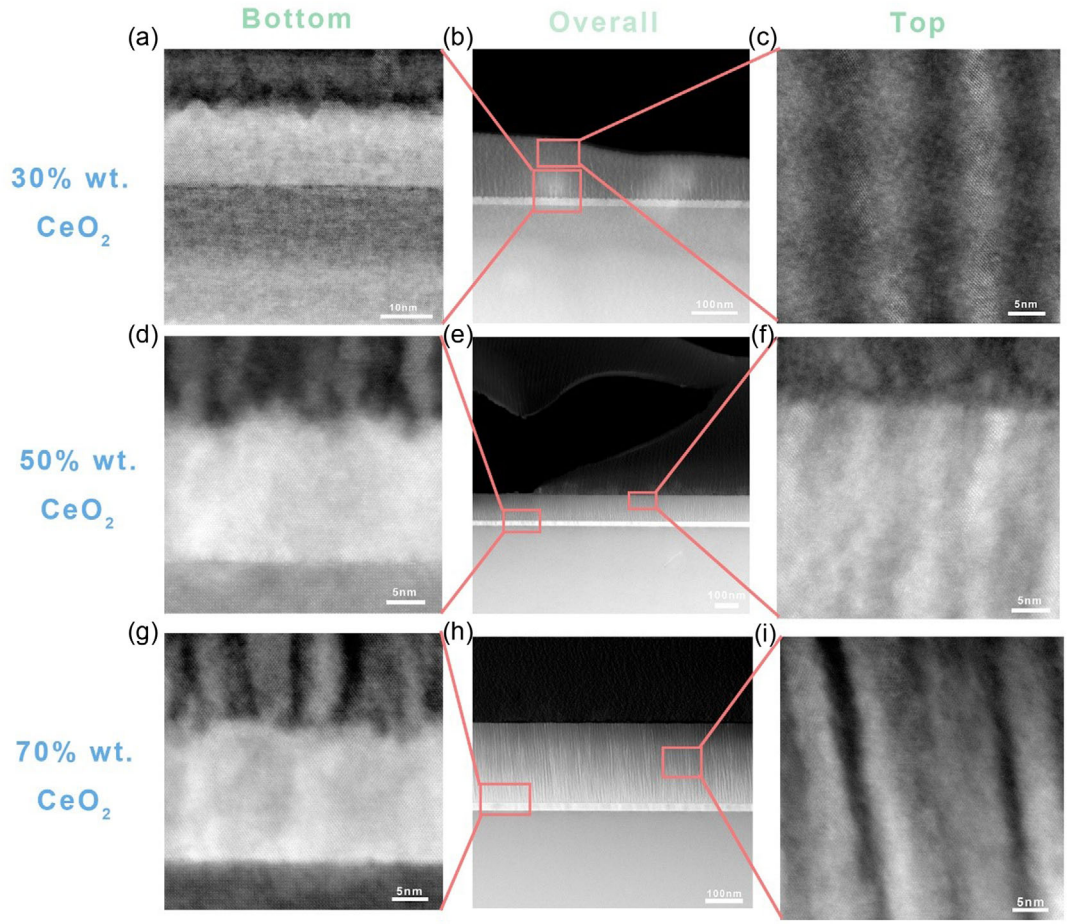

Figure 3. The cross-sectional HAADF-STEM images of SAO-CeO_2 samples before water dissolution with different ratios between SAO and CeO_2. a–c) 30 wt% CeO_2, d–f) 50 wt% CeO_2, and g–i) 70 wt% CeO_2.

Due to limitations of the testing setup, the highest temperature tested for optical permittivity is 100 °C. The optical permittivity for 50 °C and 100 °C in Figure S10c,d, Supporting Information, show similar results to the optical permittivity at room temperature.

Overall, this innovative method demonstrates that the CeO_2 nanostructure can be tuned by simply controlling the concentration ratio between CeO_2 and SAO target composition. This concentration ratio tuning is important for high surface-ratio applications, such as catalyst. Obtaining higher catalytical functions, it generally requires a high surface area to provide more active sites for the reaction to happen. Since the surface area of the CeO_2 can be easily tuned by the amount of the CeO_2 in the target composition, which can simply tune its functions for catalyst applications.[29] Beside simple CeO_2 concentration tuning demonstrated here, the thin film was deposited on a 5 mm × 10 mm STO substrate, which indicates a significant large area deposition. Further improvements to obtain even larger thin films is possible. One of the techniques to obtain large-area thin films by PLD is to conduct an off-axis deposition with rotating substrate to achieve large area deposition.[30] Previous research has shown that such water dissolution of SAO in VAN can be expanded to multiple different metal oxide systems.[3] Such material selection should be further explored with other functional oxides and other types of materials, such as nitrides. Other than exploring the additional materials to obtain similar nanostructure, resolving the mechanical instability issue of the nanowire CeO_2 is important as well. The agglomeration of the CeO_2 nanostructures is due to the very thin CeO_2 nanostructures and their high length and large aspect ratio after water dissolution. Thus, increasing the diameter and reducing the length of CeO_2 nanostructures could effectively mitigate such agglomeration issues. This can be effectively controlled by increasing the CeO_2 composition in the CeO_2:SAO nanocomposites and reducing the overall film thickness. Specifically, a larger CeO_2 composition will likely increase the CeO_2 nanopillar diameters under a low laser frequency. In addition, reducing the growth thickness from the original 108 nm to 20 nm will effectively reduce the length of the nanopillars. Such tuning in the morphology and reducing the aspect ratio of the CeO_2 nanopillars will help mitigate nanostructure agglomeration. Moreover, additional physical properties related to the in-plane strain should be further investigated in the future. The good thermal stability of the various highly textured CeO_2 nanostructures provides an opportunity for future application platforms in gas sensing and catalysis.

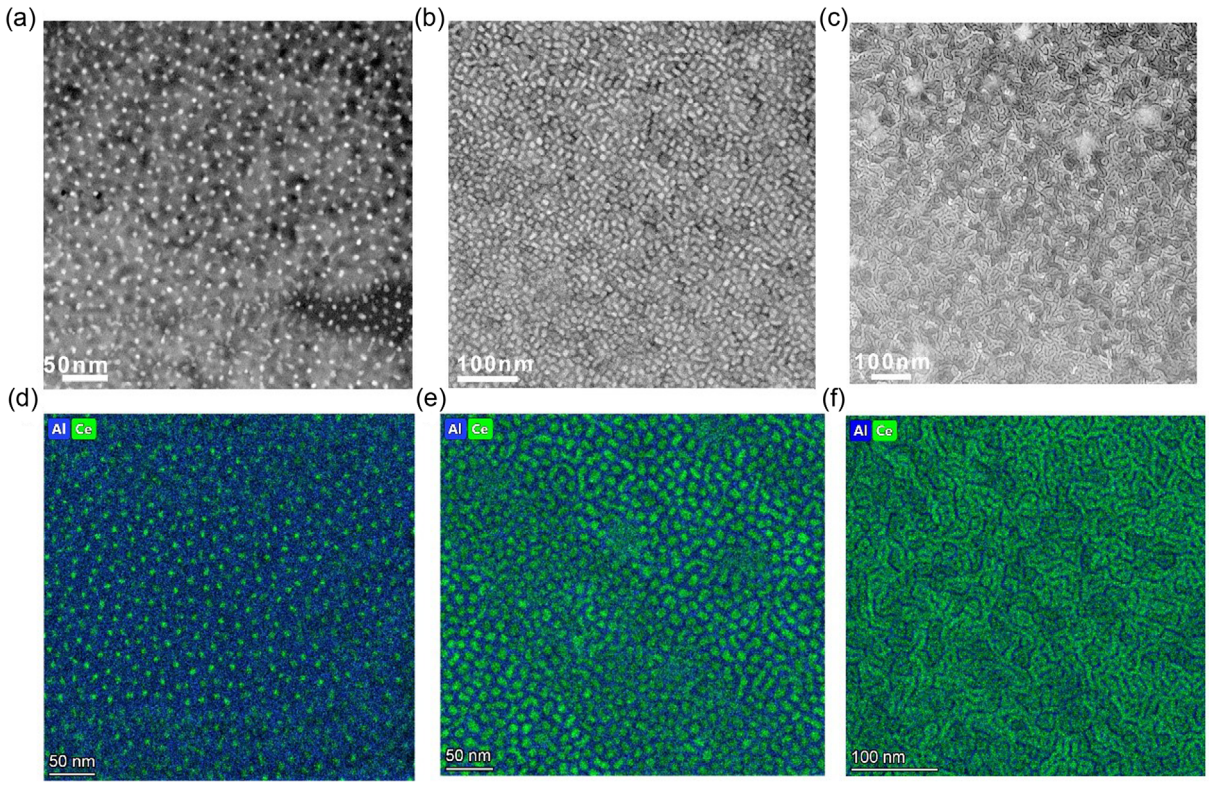

Figure 4. Plan-view of HAADF-STEM images of SAO-CeO_2 nanostructures with different concentration ratios. a) 30 wt.% CeO_2, b) 50 wt.% CeO_2, and c) 70 wt.-% CeO_2. The corresponding STEM-EDS are shown in d–f).

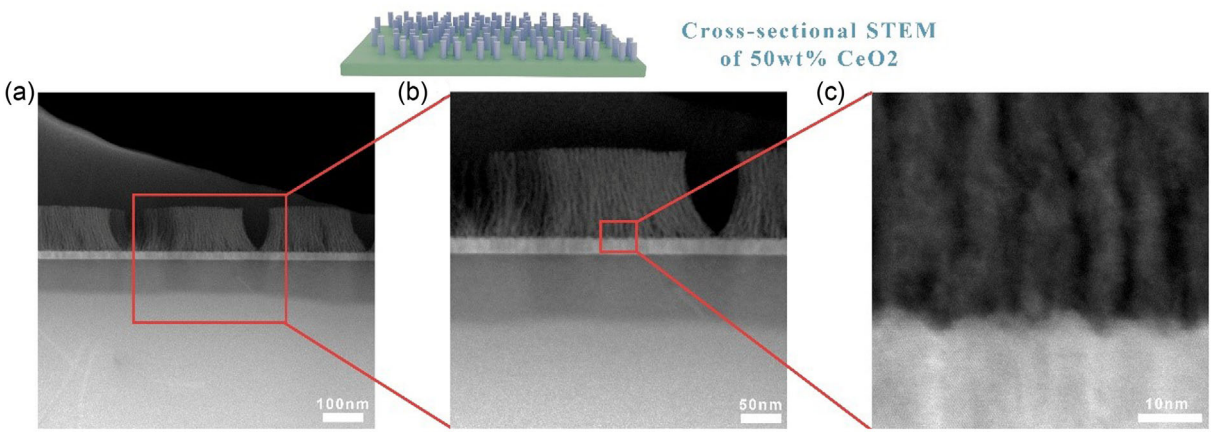

Figure 5. STEM-HAADF images of the 50 wt% of SAO-CeO_2 sample after water dissolution process. The nanostructure of CeO_2 is shown, where some of the CeO_2 nanowires agglomerate on the top.

3. Conclusion

This study presents a new method to prepare CeO_2 nanostructures using the SAO-CeO_2 VAN thin films followed by water dissolution of different concentrations of SAO within the thin films. A series of characterizations, including XRD, STEM, and AFM, were performed for the before and after water dissolution of SAO-CeO_2, and the results are presented. The resulting VAN thin films and the CeO_2 nanostructures show different morphologies after dissolving SAO, i.e., nanopillars to nanoporous structures. Thermal stability study using *in situ* XRD heating suggests the CeO_2 nanostructures are reasonability stable. Overall, this study presents a new approach via water dissolution of VAN to integrate CeO_2 nanostructures on a desired substrate towards future gas sensing, catalysis and energy devices.

4. Experimental Section

Synthesis and Dissolution Process of SAO-CeO_2 Thin Film: The $Sr_3Al_2O_6$ (SAO) target was prepared by mixing stoichiometric amounts of $SrCO_3$ and Al_2O_3. SAO was sintered in a conventional tube furnace at 1300 °C for 10 h. After sintering, the SAO was ground to a powder form. The SAO powder was then mixed with CeO_2 according to the weight percentage. The SAO-CeO_2 target was sintered in a conventional oven for another 10 h at 1300 °C.

The SAO-CeO_2 thin film was grown on $SrTiO_3$ (001) substrates using pulsed laser deposition with a KrF excimer laser (248 nm, Coherent). The laser energy was set at 420 mJ, and the laser frequency at 5 Hz. During the deposition, the temperature was set at 850 °C, and the oxygen partial pressure at 50 mtorr. Once the desired thin film was obtained, it was immersed in DI water for 12 h to ensure the SAO was fully dissolved.

Microstructure Characterization: X-ray diffraction (XRD, PANalytical Empyrean) was used to obtain the XRD patterns for all SAO-CeO_2 thin films. All cross-sectional and plan view STEM images were prepared through mechanical grinding and thinning. After the desired thickness was reached, a final polishing was performed using a Gatan Precision Ion milling system. All STEM and STEM-EDS images were acquired using a Thermo Fisher Scientific TALOS 200X TEM at 200 kV.

Supporting Information

Supporting Information is available from the Wiley Online Library or from the author.

Acknowledgements

This work is supported by the U.S. National Science Foundation (DMREF-2323752). Y.Z., C.A.M., and H.W. acknowledge the support from the U.S. National Science Foundation for the high-resolution microscopy analysis (DMR-2016453). J.S. and H.W. acknowledge the support from the U.S. Department of Energy, Office of Science, Basic Energy Sciences, under Award DE-SC0020077 for the effort on device testing. J.B. and S.Z. acknowledge the support by the U.S. Office of Naval Research (ONR, Grant No. N00014-22-1-2160). This article describes objective technical results and analysis. Any subjective views or opinions that might be expressed in the article do not necessarily represent the views of the U.S. Department of Energy, U.S. National Science Foundation, or the United States Government.

Conflict of Interest

The authors declare no conflict of interest.

Author Contributions

Benson Kunhung Tsai: conceptualization (lead); data curation (lead); formal analysis (lead); investigation (lead); methodology (lead); validation (lead); writing—original draft (lead); writing—review and editing (lead). **Jialong Huang**: investigation (supporting); methodology (supporting). **Jianan Shen**: data curation (supporting); investigation (supporting). **Yizhi Zhang**: data curation (supporting); investigation (supporting). **James P Barnard**: data curation (supporting); investigation (supporting). **Claire A Mihalko**: data curation (supporting); investigation (supporting). **Abhijeet Choudhury**: data curation (supporting); investigation (supporting). **Shiyu Zhou**: data curation (supporting); investigation (supporting). **Haiyan Wang**: conceptualization (lead); funding acquisition (lead); investigation (lead); project administration (lead); resources (lead); supervision (lead); writing—review and editing (lead).

Data Availability Statement

The data that support the findings of this study are available in the supplementary material of this article.

Keywords

1D nanomaterials, nanoporous thin films, nanostructured CeO_2, thermal stability, vertically aligned nanocomposites

Received: February 23, 2025
Revised: June 2, 2025
Published online:

[1] D. Voiry, H. S. Shin, K. P. Loh, M. Chhowalla, *Nat. Rev. Chem.* **2018**, *2*, 0105.
[2] M. Kahl, E. Voges, S. Kostrewa, C. Viets, W. Hill, *Sens. Actuators, B* **1998**, *51*, 285.
[3] Y. S. Kim, J. Song, C. Hwang, X. Wang, H. Wang, J. L. MacManus-Driscoll, H.-K. Song, S. Cho, *Adv. Sci.* **2018**, *5*, 1800851.
[4] Z. Cai, B. Liu, X. Zou, H.-M. Cheng, *Chem. Rev.* **2018**, *118*, 6091.
[5] K. Nielsch, J. Choi, K. Schwirn, R. B. Wehrspohn, U. Gösele, *Nano Lett.* **2002**, *2*, 677.
[6] A. L. Sangle, S. Singh, J. Jian, S. R. Bajpe, H. Wang, N. Khare, J. L. MacManus-Driscoll, *Nano Lett.* **2016**, *16*, 7338.
[7] J. Kašpar, P. Fornasiero, N. Hickey, *Catal. Today* **2003**, *77*, 419.
[8] T. Montini, M. Melchionna, M. Monai, P. Fornasiero, *Chem. Rev.* **2016**, *116*, 5987.
[9] a) S.-Y. Jeong, Y. K. Moon, J. Wang, J.-H. Lee, *Nat. Commun.* **2023**, *14*, 233; b) X. Q. Fu, C. Wang, H. C. Yu, Y. G. Wang, T. H. Wang, *Nanotechnology* **2007**, *18*, 145503.
[10] a) P. Pal, S. K. Pahari, A. Sinhamahapatra, M. Jayachandran, G. V. M. Kiruthika, H. C. Bajaj, A. B. Panda, *RSC Adv.* **2013**, *3*, 10837; b) C. Sun, H. Li, Z. Wang, L. Chen, X. Huang, *Chem. Lett.* **2004**, *33*, 662; c) T. Yu, J. Joo, Y. I. Park, T. Hyeon, *Angew. Chem. Int. Ed.* **2005**, *44*, 7411.
[11] R.-J. La, Z.-A. Hu, H.-L. Li, X.-L. Shang, Y.-Y. Yang, *Mater. Sci. Eng.: A* **2004**, *368*, 145.
[12] a) X. Wang, H. Wang, *Chemosensors* **2021**, *9*, 145; b) J. Song, H. Wang, *J. Phys.: Mater.* **2025**, *8*, 012002.
[13] J. Huang, L. Li, Z. Hu, B. K. Tsai, J. Huang, J. Shen, Y. Zhang, J. P. Barnard, J. Song, H. Wang, *Nano Lett.* **2024**, *24*, 10081.
[14] J. Huang, A. Gellatly, A. Kauffmann, X. Sun, H. Wang, *Cryst. Growth Des.* **2018**, *18*, 4388.
[15] D. Zhang, S. Misra, L. Li, X. Wang, J. Jian, P. Lu, X. Gao, X. Sun, Z. Qi, M. Kalaswad, X. Zhang, H. Wang, *Adv. Opt. Mater.* **2020**, *8*, 1901359.
[16] A. Chen, Z. Bi, C.-F. Tsai, J. Lee, Q. Su, X. Zhang, Q. Jia, J. L. MacManus-Driscoll, H. Wang, *Adv. Funct. Mater.* **2011**, *21*, 2423.
[17] J. Huang, X. L. Phuah, L. M. McClintock, P. Padmanabhan, K. S. N. Vikrant, H. Wang, D. Zhang, H. Wang, P. Lu, X. Gao, X. Sun, X. Xu, R. Edwin García, H.-T. Chen, X. Zhang, H. Wang, *Mater. Today* **2021**, *51*, 39.
[18] J. Huang, J. L. MacManus-Driscoll, H. Wang, *J. Mater. Res.* **2017**, *32*, 4054.
[19] J. Huang, H. Wang, Z. Qi, P. Lu, D. Zhang, B. Zhang, Z. He, H. Wang, *Nano Lett.* **2021**, *21*, 1032.
[20] S. Misra, H. Wang, *Mater. Horiz.* **2021**, *8*, 869.
[21] X. Sun, J. L. MacManus-Driscoll, H. Wang, *Annu. Rev. Mater. Res.* **2020**, *50*, 229.

[22] J. Lu, D. Zhang, R. L. Paldi, Z. He, P. Lu, J. Deitz, A. Ahmad, H. Dou, X. Wang, J. Liu, Z. Hu, B. Yang, X. Zhang, A. A. El-Azab, H. Wang, *Mater. Horiz.* **2023**, *10*, 3101.
[23] a) J. Huang, Z. Qi, L. Li, H. Wang, S. Xue, B. Zhang, X. Zhang, H. Wang, *Nanoscale* **2018**, *10*, 17182; b) D. Lu, D. J. Baek, S. S. Hong, L. F. Kourkoutis, Y. Hikita, Harold Y. Hwang, *Nat. Mater.* **2016**, *15*, 1255.
[24] B. K. Tsai, J. Song, J. Liu, J. Shen, Y. Zhang, X. Zhang, H. Wang, *Next Nanotechnology* **2024**, *6*, 100071.
[25] C. Balaji Gopal, M. García-Melchor, S. C. Lee, Y. Shi, A. Shavorskiy, M. Monti, Z. Guan, R. Sinclair, H. Bluhm, A. Vojvodic, W. C. Chueh, *Nat. Commun.* **2017**, *8*, 15360.
[26] a) H. Li, Y. Qu, X. Zhang, *Inorg. Chem. Commun.* **2021**, *130*, 108692; b) Q. Hu, B. Huang, Y. Li, S. Zhang, Y. Zhang, X. Hua, G. Liu, B. Li, J. Zhou, E. Xie, Z. Zhang, *Sens. Actuators, B* **2020**, *307*, 127638.
[27] J. Yoon, S. Cho, J.-H. Kim, J. Lee, Z. Bi, A. Serquis, X. Zhang, A. Manthiram, H. Wang, *Adv. Funct. Mater.* **2009**, *19*, 3868.
[28] a) G. Mussabek, V. Lysenko, D. Yermukhamed, V. Sivakov, V. Yu, *Results Phys.* **2020**, *18*, 103258; b) M. Košiček, J. Zavašnik, O. Baranov, B. Šetina Batič, U. Cvelbar, *Cryst. Growth Des.* **2022**, *22*, 6656.
[29] a) J. Lee, P. Tieu, J. Finzel, W. Zang, X. Yan, G. Graham, X. Pan, P. Christopher, *JACS Au* **2023**, *3*, 2299; b) W. Kang, D. O. Ozgur, A. Varma, *ACS Appl. Nano Mater.* **2018**, *1*, 675.
[30] J. A. Greer, M. D. Tabat, *J. Vac. Sci. Technol., A* **1995**, *13*, 1175.

